LA-UR- 09-00406

Title: A Novel Synthetic Aperture Technique for Breast Tomography with Toroidal Arrays

Author(s): Lianjie Huang, EES-17
Francesco Simonetti, Imperial College London

Intended for: Proceedings of 2009 SPIE Medical Imaging

A Novel Synthetic Aperture Technique for Breast Tomography with Toroidal Arrays

F. Simonetti [a,b], L. Huang [b]

[a]Department of Mechanical Engineering, Imperial College, SW7 2AZ, London, UK;
[b]MS D443, Los Alamos National Laboratory, Los Alamos, NM 87545, USA

ABSTRACT

Ultrasound is commonly used as an adjunct to mammography for diagnostic evaluation of suspicions arising from breast cancer screening. As an alternative to conventional sonography that uses hand-held transducers, toroidal array probes that encircle the breast immersed in a water bath have been investigated for ultrasound tomography. This paper introduces a new method for three-dimensional synthetic aperture diffraction tomography that maximizes the resolution in the scanning direction and provides quantitative reconstructions of the acoustic properties of the object. The method is validated by means of numerical simulations.

Keywords: Ultrasound Tomography, Synthetic Aperture, Arrays, Breast

1. INTRODUCTION

With an estimated 1.15 million new cases each year, breast cancer is by far the most common cancer among women throughout the world. Randomized clinical trials performed in the USA and UK, have demonstrated a 25% to 35% reduction in breast cancer mortality in women 50-69 years who are screened annually or biennially[1] highlighting the key role of screening that is currently based on the gold standard of X-ray mammography.

The sensitivity and specificity of mammography depend on the personal characteristics of individual patients and are determined by the working principle of mammography. In fact, a mammogram is an X-ray projection of the mass density distribution inside the volume of a breast squeezed between two plates. The diagnosis of cancer is based on detection of calcium deposits (high density) and the presence of abnormal masses. In radiographically dense breasts, sensitivity can be as low as 30 to 48% because the normal breast parenchyma masks the presence of masses. Dense breast tissue is common: approximately 50% of women younger than 50 years and a third of older women have dense parenchyma.[2] This explains why the sensitivity of mammography is low in young premenopausal women and those who receive hormonal replacement therapy HRT. The same considerations apply to specificity that tends to be lower in women with a low body mass index.[3] As a result, the positive predictive value or PPV (the probability of having cancer for a woman with a positive test) ranges from 20% in women under age 50 to 60% to 80% in women aged 50-69. A PPV of 20% means that 80% of the abnormal findings with mammography are not related to cancer. The low PPV and the increased risk of developing cancer due to ionizing radiation, have limited the use of mammography screening in younger women. Currently mammography is only recommended for women aged between 50-70 years[4] in the UK.

To improve the sensitivity and specificity of mammography, ultrasound is now commonly used as an adjunct to mammography for diagnostic evaluation of suspicions arising from mammograms, particularly for women with dense breasts.[5] In fact, while mammography is sensitive to density variations only, ultrasound can also differentiate between structures that have the same density but different elastic properties that result in changes in sound speed and acoustic impedance. The possibility of using ultrasound for screening is being investigated within the ongoing American College of Radiology Imaging Network (ACRIN) trial 6666 (http://www.acrin.org). This is the largest trial in which sonography and mammography have been performed and read independently to allow the analysis of the performance of each modality separately and in combination. Preliminary results[6] have confirmed that adding single screening sonography to mammography increases the detection of cancer in women with dense breasts, showing masses invisible on mammograms. However, if used alone, screening with ultrasound leads to a high rate of false positives with PPV 10%. The same work has pointed out that the low PPV is related to the operator dependence of freehand ultrasound screening. Operator dependence can become a barrier to the widespread use of screening ultrasound because of a shortage of qualified personnel, the need for

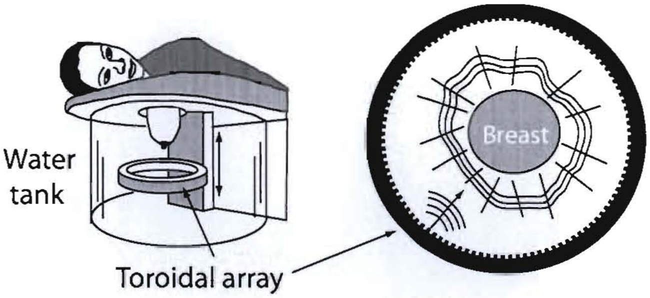

Figure 1. Typical configuration for breast ultrasound tomography. The breast is pendulant in a water bath. A toroidal ultrasound array encircles the breast and is moved vertically to scan its volume.

complex scanning protocols and costs associated with the time required to perform bilateral scans. The same report has also stressed that diagnostic uncertainty regarding complex cysts remains a major source of false positive results and suggests that the uses of quantitative techniques such as elastography could improve the specificity of ultrasound screening. Other factors that prevent the use of ultrasound screening are the presence of speckle noise and image artifacts that can mask smaller lesions, thus reducing sensitivity.

In order to overcome the limitations of conventional sonography, the possibility of developing ultrasound into an automated tomography modality has been investigated since early 1970s.[7–9] This approach is aimed at producing images of the breast comparable to those obtained with high resolution X-ray or CT but without the risks associated with ionizing radiation and at a much lower cost. The CURE[10] prototype and the system developed by Andre et al.[11] are examples of ultrasound tomography setups for breast imaging. Instead of scanning the breast with a freehand probe, a patient is lying prone on a table with a breast suspended in a water bath through an aperture in the table, Fig. 1. A toroidal array probe then encircles the breast and is scanned vertically to sweep the entire volume of the breast. At each array position, the breast is insonified from all possible angles in the plane of the array and the backscattered and transmitted ultrasonic fields through the breast are measured by all the array elements in parallel and for each insonification. These measurements are subsequently used by a tomography algorithm to reconstruct a slice across the breast in the plane of the array. This results in a fully automated scanning procedure that does not require highly trained sonographers and the compression of the breast that is known to cause apprehension in women undergoing mammography.[12] Different algorithms have been proposed to reconstruct a slice across the breast, such as travel time tomography[7,9,10] and diffraction tomography.[13] These methods reconstruct a slice from the measurements performed by the array at a particular position, and assume that the array *'sees'* the slice corresponding to the plane of the array only. However, since the incident field spreads out from the plane of the array, the measurements also depend on the structures of the breast that are outside the plane of the array. This can cause image artifacts and reduces the resolution in the direction perpendicular to the array, thus increasing the so-called slice thickness.

This paper introduces a new imaging algorithm for three-dimensional diffraction tomography that provides the image of a particular slice across the object by combining measurements performed at multiple vertical positions of the array. In particular, we exploit the idea of Synthetic Aperture Radar (SAR), whereby an image of the surface of the Earth is obtained by combining the microwave signals recorder as an aircraft flies over the surface, see for instance Ref.[14] Our Synthetic Aperture Diffraction Tomography (SADT) method is aimed at increasing the resolution in the direction of the scanning thus limiting the thickness of each slice.

The paper begins by establishing the link between the measurements and the structure of the object represented in the spatial frequency domain in Sec. 2. The reconstruction algorithm is subsequently presented in Sec. 3 and validated by means of a numerical example in Sec. 4.

2. MEASUREMENTS AND OBJECT'S STRUCTURE

Let us consider a complex three-dimensional object that occupies a volume D in the space denoted by a Cartesian coordinate system $\{O, x_1, x_2, x_3\}$ as shown in Fig. 2(a). The object is mathematically described by the so-called

'Object Function,' $O(\mathbf{r})$, of support D that is linked to the speed of sound and attenuation coefficient.[15] For a lossless object

$$O(\mathbf{r}) = k^2\left[\left(\frac{c_0}{c(\mathbf{r})}\right)^2 - 1\right], \tag{1}$$

where $k = 2\pi/\lambda$ is the wavenumber, λ the wavelength, c_0 the sound speed of the homogeneous background in which the object is immersed and $c(\mathbf{r})$ the local sound speed inside the object. Therefore, if the function $O(\mathbf{r})$ can be reconstructed from scattering measurements, the sound speed map across the object can be obtained by inverting (1).

Here, we assume that the object is illuminated with a monochromatic plane wave propagating in the direction $\hat{\mathbf{r}}_0$ and the scattered field is observed in the direction $\hat{\mathbf{r}}$. Moreover, it is assumed that these measurements can be performed with a toroidal array (Fig. 2a) whose vertical position is defined by the elevation angle ψ (Fig. 2a). As a result, the unit vectors $\hat{\mathbf{r}}_0$ and $\hat{\mathbf{r}}$, are fully defined by the angle pairs (θ, ψ) and (ϕ, ψ), respectively. This model is sufficiently accurate if the array elements are small compared to the wavelength (since each transmitter can be considered as a 3-D point source) and if the object is much smaller than the array radius, since the field reaching the object can be approximated by a plane wave.

Let $f(\phi, \theta, \psi)$ define the scattering amplitude[16] measured as the array is scanned vertically. To simplify the mathematical treatment it is assumed that $\psi \in [0, \pi]$, i. e. the array is scanned from $x_3 = \infty$ to $-\infty$. In addition, for each position of the array all the transmit-receive pairs are measured, i. e. $\phi, \theta \in [0, 2\pi]$. The fundamental Fourier diffraction theorem,[17] demonstrates that the scattering amplitude corresponding to a particular illumination and detection pair, $f(\hat{\mathbf{r}}_0, \hat{\mathbf{r}})$, provides the spatial fourier transform of $O(\mathbf{r})$, $\tilde{O}(\mathbf{K})$, at the spatial frequency $K = k(\hat{\mathbf{r}} - \hat{\mathbf{r}}_0)$, i.e.

$$f(\hat{\mathbf{r}}_0, \hat{\mathbf{r}}) = \tilde{O}[k(\hat{\mathbf{r}} - \hat{\mathbf{r}}_0]. \tag{2}$$

Therefore, if scattering measurements could be performed for all possible pairs $\hat{\mathbf{r}}_0$ and $\hat{\mathbf{r}}$ the function $\tilde{O}(\mathbf{K})$ would be reconstructed for all the spatial frequencies within a ball of radius $2k$ also known as the Ewald Limiting Spehre[17] (ELS). As a result, the object function $O(\mathbf{r})$ could be retrieved by performing the inverse fourier transform of the reconstructed $\tilde{O}(\mathbf{K})$ assuming that it vanishes outside the ELS. This would lead to a low-pass filtered reconstruction of the object function containing spatial frequencies larger than $\lambda/2$ according to the classical resolution limit*. However, in order to measure the scattering amplitude for all possible illumination and detection directions, the array sensors should be distributed over a sphere that contains the object. Obviously

---

*Note that the same conclusion can be reached under the Rytov approximation.[15]

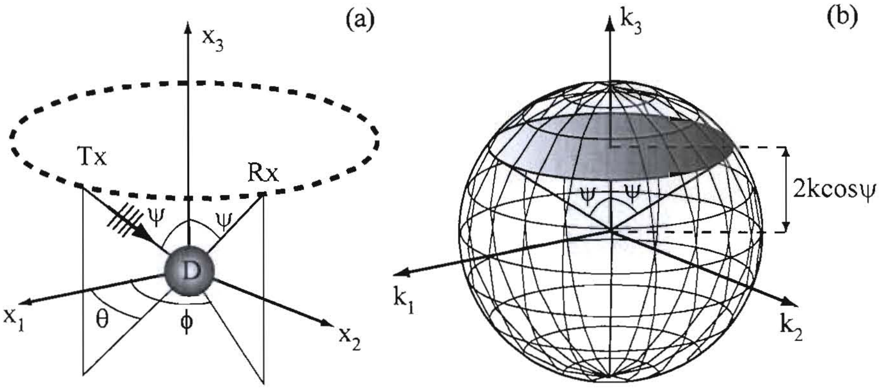

Figure 2. Mapping between SADT measurements and the spatial frequency domain. (a) Diagram of the measurement setup, a toroidal array is scanned vertically and at each position all the transmit-receive pairs are recorded; (b) Spatial frequency space, showing the Ewald Limiting Sphere of radius $2k$.

this is not possible for *in vivo* breast imaging. Moreover, the number of sensors required to avoid aliasing would be beyond the capability of current ultrasound technology.

Here, we show that the measurements performed by scanning the toroidal array can lead to the full coverage of the ELS despite the fact that not all the $\hat{\mathbf{r}}_0$ and $\hat{\mathbf{r}}$ pairs are available. When the array is at the vertical position defined by the elevation ψ, the components of the spatial frequency vector, $k(\hat{\mathbf{r}} - \hat{\mathbf{r}}_0)$, are

$$\begin{aligned} K_1 &= k \sin\psi(\cos\phi - \cos\theta), &(3)\\ K_2 &= k \sin\psi(\sin\phi - \sin\theta), &(4)\\ K_3 &= 2k\cos\psi. &(5) \end{aligned}$$

Therefore, for a particular array position, ψ, as the (θ, ϕ) pairs vary in the interval $[0, \pi] \times [0, \pi]$ the measurements populate a disk of the K-space, contained in the plane $K_3 = 2k\cos\psi$ and with radius $2k\sin\psi$ as shown in Fig. 2(b). As a result, by scanning the array vertically the entire ELS can be filled. This implies that the measurements performed in this fashion are sufficient to reconstruct the object function as in the ideal case of a spherical array of sensors. Importantly, spatial frequencies as high as $2k$ can be retrieved in the scanning direction, leading to an axial resolution limit of $\lambda/2$.

3. SYNTHETIC APERTURE DIFFRACTION TOMOGRAPHY

The SADT algorithm proposed in this paper consists of two steps. First a Synthetic Aperture Beamforming (SABF) image of the object is produced. Subsequently, the SADT image is obtained from the SABF one by deconvolution with the point spread function (PSF) of SABF. For this purpose, we introduced the SABF algorithm first.

3.1 Synthetic Aperture Beamforming

Let $\mathbf{z}$ be a point in the image space, we define the beamforming functional as

$$\mathfrak{I}_{BF}(\mathbf{z}) = \int_0^{\pi} d\psi \int_0^{2\pi} d\theta \int_0^{2\pi} d\phi \exp[ik\hat{\mathbf{u}}(\phi,\psi)\cdot\mathbf{z}] f(\phi,\theta,\psi) \exp[ik\hat{\mathbf{u}}(\theta,\psi)\cdot\mathbf{z}], \tag{6}$$

where $\hat{\mathbf{u}}$ is the unit vector. The second exponential in eq. (6) represents focussing in transmission while the first corresponds to the focussing of the received signal as discussed in Ref.[18] for the 2-D case. The PSF associated with the functional (6) can be obtained by considering the image of a point scatterer at position $\mathbf{r}$. In this case the scattering amplitude is

$$f(\phi,\theta,\psi) = \exp\{-ik[\hat{\mathbf{u}}(\theta,\psi) + \hat{\mathbf{u}}(\phi,\psi)]\cdot\mathbf{r}\}, \tag{7}$$

and the PSF reads

$$h(\mathbf{z},\mathbf{r}) = \int_0^{\pi} d\psi \int_0^{2\pi} d\theta \int_0^{2\pi} d\phi \exp\{ik\hat{\mathbf{u}}(\phi,\psi)\cdot[\mathbf{z}-\mathbf{r}]\} \exp\{ik\hat{\mathbf{u}}(\theta,\psi)\cdot[\mathbf{z}-\mathbf{r}]\}. \tag{8}$$

This is space invariant since it depends on $\mathbf{z} - \mathbf{r}$ rather than the individual variables $\mathbf{z}$ and $\mathbf{r}$. As a result, the SABF image is the convolution of the object function with the PSF. To evaluate the PSF let $\mathbf{a} = \mathbf{z} - \mathbf{r}$. Expression (8) can be rewritten in the form

$$h(\mathbf{a}) = \int_0^{\pi} d\psi \exp(i2k\cos\psi a_\perp) \int_0^{2\pi} d\theta \exp[ik\hat{\mathbf{u}}_{||}(\theta,\psi)\cdot\mathbf{a}_{||}] \int_0^{2\pi} d\phi \exp[ik\hat{\mathbf{u}}_{||}(\phi,\psi)\cdot\mathbf{a}_{||}], \tag{9}$$

where the subscript $||$ and $\perp$ refer to the components of a vector in the plane $x_3 = 0$ and along $\hat{\mathbf{u}}_3$, respectively. By using the Jacobi-Anger expansion the integral in (9) becomes

$$h(\mathbf{a}) = 4\pi^2 \int_0^{\pi} d\psi \exp(i2k\cos\psi a_\perp) J_0^2(k\sin\psi a_{||}), \tag{10}$$

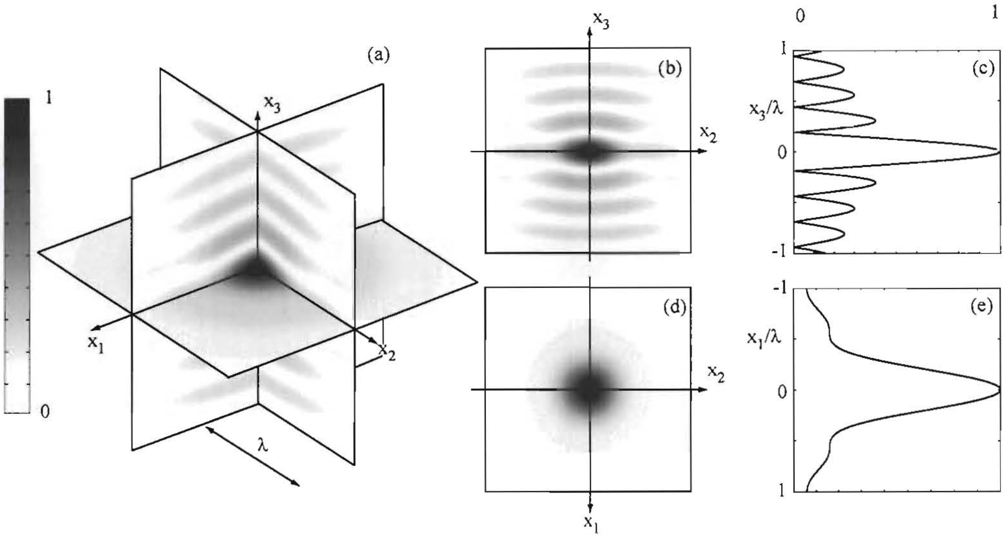

Figure 3. Normalized PSF for the SABF method. The gray scale represents the amplitude distribution across a plane. (a) 3-D views of the PSF across three orthogonal planes; (b) $x_1 = 0$ plane; (c) profile along the $\hat{\mathbf{x}}_3$ axis; (d) $x_3 = 0$ plane; (e) profile along the $\hat{\mathbf{x}}_1$ axis.

where J_0 is the Bessel function of the first kind of zero order. Since J_0 is even and $\cos\psi$ is odd, the integral in (10) is equivalent to

$$h(\mathbf{a}) = 8\pi^2 \int_0^{\pi/2} d\psi \cos(\alpha\cos\psi) J_0^2(\beta\sin\psi), \tag{11}$$

with $\alpha = 2ka_\perp$ and $\beta = ka_\parallel$. Equation (11) implies that the PSF is real. By using the series expansion of J_0^2 and the Bessel second integral,[19] the integral in (11) can be evaluated as a series of Bessel functions of the first kind, J_m, i. e.

$$h(\mathbf{a}) = 4\pi^3 \sum_{m=0}^{+\infty} \frac{(-1)^m}{(m!)^2} \binom{2m}{m} \left(\frac{\beta}{4}\sqrt{\frac{2}{\alpha}}\right)^{2m} J_m(\alpha), \tag{12}$$

where $\binom{2m}{m}$ are the binomial coefficients.

The three-dimensional structure of the normalized PSF is shown in Fig. 3. As it can be deduced from (12) the PSF is symmetric relative to the $\hat{\mathbf{x}}_3$ axis (Fig. 3d) and is described by the function $4\pi^2 J_0(2kx_3)$ along it (Fig. 3c). If the resolution in the direction $\hat{\mathbf{x}}_3$ is defined by considering the first null of the PSF, according to the Rayleigh criterion, the resolution limit becomes 0.19λ at the expenses of large sidelobes. On the other hand, the sidelobes are lower in the plane $x_3 = 0$; however, the width of the central lobe is now larger, Fig. 3(e).

3.2 SADT algorithm

The algorithm for SADT imaging consists of the following steps:

- Define a 3-D cubic grid of points that covers the volume to be imaged;
- Calculate the SABF functional at each point of the grid using (4);
- Deconvolution. This is achieved in the spatial frequency domain dividing the 3-D FFT of the SABF image by the 3-D FFT of the PSF and performing the inverse 3-D FFT. The PSF is evaluated numerically by means of (12).

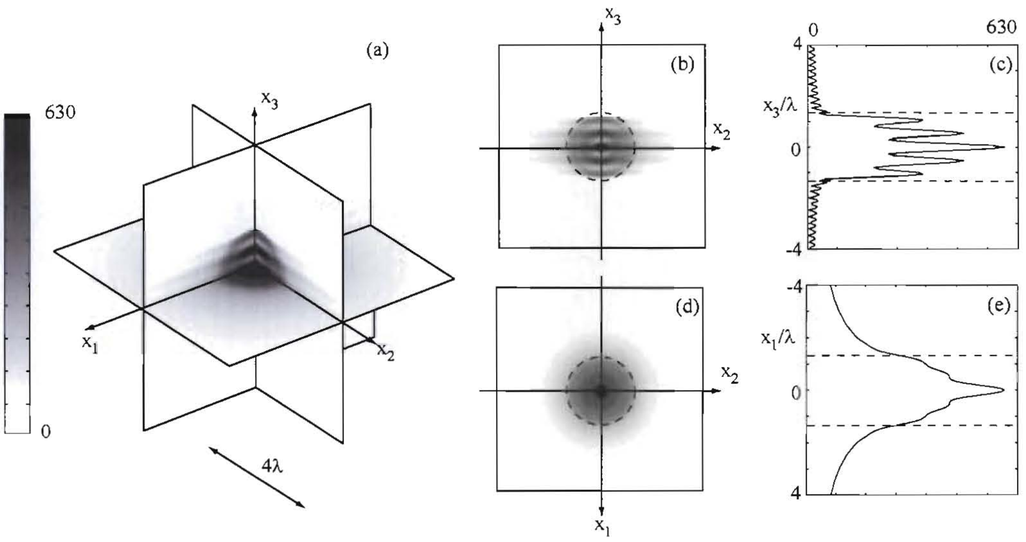

Figure 4. SABF image of the sphere. The gray scale represents the amplitude distribution of the beamforming functional across a plane. (a) 3-D views across three orthogonal planes; (b) $x_1 = 0$ plane; (c) profile along the $\hat{\mathbf{x}}_3$ axis; (d) $x_3 = 0$ plane; (e) profile along the $\hat{\mathbf{x}}_1$ axis.

It should be observed that as long as the imaging grid is uniform there is no need for data interpolation techniques as required by other diffarction tomography algorithms.

4. NUMERICAL SIMULATIONS

In order to illustrate the SADT method, the problem of reconstructing the speed of sound distribution inside a homogeneous sphere is considered. In this case the forward scattering can be predicted with a semi-analytic formula, see for instance Ref.[20] The speed of sound inside the sphere is $c = 1485m/s$ and is immersed in water ($c_0 = 1500m/s$); no density contrast is considered. The radius of the sphere is 20 mm and is insonified by plane waves at 100 KHz, i.e. $\lambda = 15mm$. The toroidal array consists of $N = 80$ point-like transducers and measurements are performed over 79 vertical positions. The vertical positions are selected so as to achieve a constant elevation interval $\Delta\psi = \pi/N$. The imaging volume is a cube 248mm in size and divided into 1mm cubic voxels.

Figure 4 shows the three-dimensional SABF image of the sphere. Due to the anisotropy of the PSF, the reconstruction of the sphere is not homogeneous as it is clearly seen in Figs 4(b) and 4(d) that are two cross sections in the vertical and horizontal planes passing through the origin. The reconstruction along the $\hat{\mathbf{x}}_3$ axis (Fig. 4c) is sharper than in the $x_3 = 0$ plane (Fig. 4e); however, it contains more artifacts. The higher resolution is due the narrow central lobe of the PSF along the $\hat{\mathbf{x}}_3$ axis (compare Fig. 3c and 3e). On the other hand, the artifact peaks seen in Fig. 4(c) are due to the sidelobes of the PSF which are larger along the $\hat{\mathbf{x}}_3$ axis than those in the $x_3 = 0$ plane (compare Fig 3c, and 3e).

Next Fig. 5 is the SADT reconstruction of the object function obtained following the method outlined in Sec. 3.2. SADT leads to a more homogeneous reconstruction of the sphere especially along the $\hat{\mathbf{x}}_3$ axis. Moreover, the image is sharper as it can be seen in the cross sections in Figs 5(c) and 5(e) and also provides an accurate reconstruction of the sphere shape. However, the strong central artifact that was present in the SABF images remains. The velocity map can be derived by means of eq. (1) and its profile along the $\hat{\mathbf{x}}_1$ axis is shown in Fig. 6.

5. CONCLUSIONS

We have proposed a new method for ultrasound tomography of complex three-dimensional objects by means of a toroidal array of point-like sensors that encircles the object. In particular, we have demonstrated that by

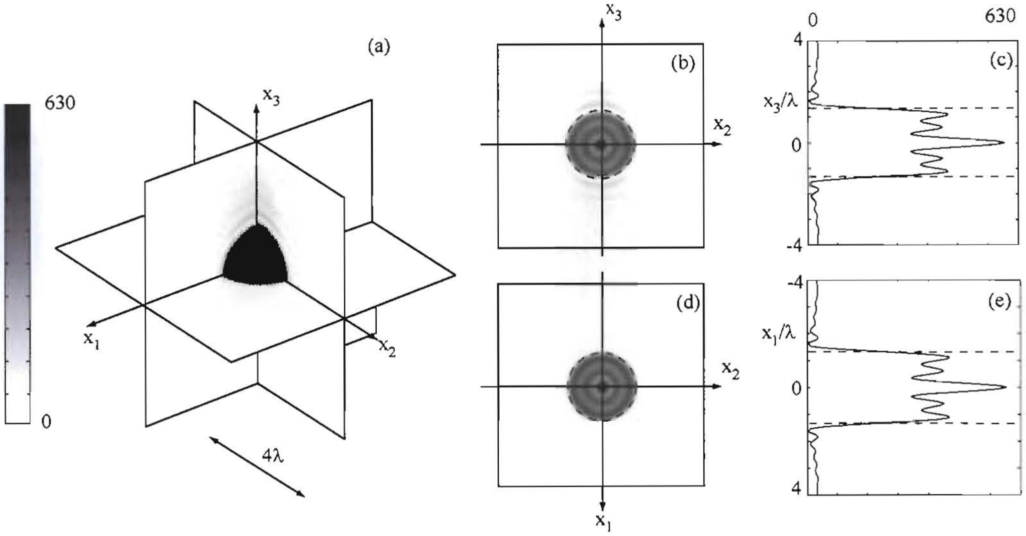

Figure 5. Object function reconstructed with the SADT method. (a) 3-D views across three orthogonal planes; (b) $x_1 = 0$ plane; (c) profile along the $\hat{\mathbf{x}}_3$ axis; (d) $x_3 = 0$ plane; (e) profile along the $\hat{\mathbf{x}}_1$ axis.

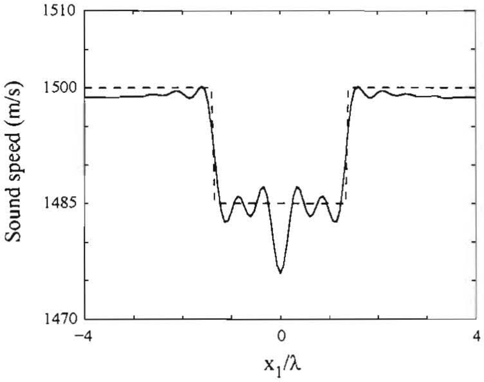

Figure 6. Actual (dashed line) and reconstructed (solid line) velocity profile along the $\hat{\mathbf{x}}_1$ axis.

scanning the array across the volume of the object, a full coverage of the Ewald Limiting Sphere can be achieved. This implies that the measurements obtained by scanning the array are sufficient to reconstruct the object structure with the same degree of accuracy as full-view diffraction tomography that requires the array sensors to be distributed over a sphere that contains the object. This leads to the concept of Synthetic Aperture Diffraction Tomography (SADT). Noticeably, SADT achieves the theoretical $\lambda/2$ resolution limit in the scanning direction, thus limiting the slice thickness. Moreover, SADT is more attractive than full-view diffraction tomography as it reduces the number of array elements required to avoid aliasing, hence the complexity of the hardware, and limits the size of the datasets to be processed.

The method has been validated numerically by reconstructing the sound speed distribution inside a homogeneous fluid sphere immerse in water leading to an accurate shape reconstruction and a satisfactory representation of the sound speed distribution inside the sphere.

Finally the practical implementation of SADT requires the use of an array with elements that are much smaller than the wavelength. In fact, each element should insonify planes that are at a large distance from the array and receive signals scattered from points outside the plane of the array. This poses a significant engineering challenge because as the size of the elements decreases the radiation efficiency drops and the electrical impedance increases. These two factors combined together tend to reduce the overall signal-to-noise ration and could affect the overall performance of SADT.

ACKNOWLEDGMENTS

This work was supported through the U. S. DOE Laboratory Directed Research and Development program at Los Alamos National Laboratory. FS is also grateful to the UK Royal Academy of Engineering / EPSRC for the support received.

REFERENCES

[1] Berry, D. A., Cronin, K. A., Plevritis, S., and et al., "Effect of screening and adjuvant therapy on mortality," *N. Eng. J. Med* **353**, 1748–1759 (2005).

[2] Stomper, P. C., D'Souza, D. J., Dinitto, P. A., and et al., "Analysis of parenchymal density on mammograms in 1353 women 25-79 years old," *AJR Am J Roentgenol* **167**, 1261–1265 (1996).

[3] Banks, E., Reeves, G., Beral, V., and et al., "Influence of personal characteristics of individual women on sensitivity and specificity of mammography in the million women study: cohort study.," *BMJ* **329**, 329–477 (2004).

[4] Advisory Committee on Breast Cancer Screening, [*Screening for breast cancer in England: Past and future*], vol. 61, NHSBSP Publication, London (2006).

[5] Kolb, T. M., Lichy, J., and Newhouse, J. H., "Comparison of the performance of screening mammography, physical examination, and breast us and evaluation of factors that influence them: An analysis of 27,825 patient eveluation," *Radiology* **225**, 165–175 (2002).

[6] Berg, W. A., Blume, J. D., Cormack, J. B., and et al., "Combined screening with ultrasound and mammography vs mammography alone in women at elevated risk of breast cancer," *JAMA* **299**, 2151–2163 (2008).

[7] Greenleaf, J. F., Johnson, S. A., Lee, S. L., Herman, G. T., and Wood, E. H., "Algebraic reconstruction of spatial distributions of acoustic absorption within tissue from their two-dimensional acoustic projections," in [*Acoustical Holography*], Green, P. S., ed., **5**, 591–603, Plenum Press, New York (1973).

[8] Greenleaf, J. F., Johnson, S. A., Samayoa, W. F., and Duck, F. A., "Algebraic reconstruction of spatial distributions of acoustic velocities in tissue from their time-of-flight profiles," in [*Acoustical Holography*], Green, P. S., ed., **6**, 71–90, Plenum Press, New York (1975).

[9] Carson, P. L., Meyer, C. R., Scherzinger, A. L., and Oughton, T. V., "Breast imaging in coronal planes with simultaneous pulse echo and transmission ultrasound," *Science* **214**(4), 1141–1143 (1981).

[10] Duric, N., Littrup, P. Poulo, L., Babkin, A., Pevzner, R., Holsapple, E., Rama, O., and Glide, C., "Detection of breast cancer with ultrasound tomography: First results with the computed ultrasound risk evaluation (cure) prototype," *Med. Phys.* **34**(2), 773–785 (2007).

[11] Andre, M. P., Janee, H. S., M. P., Otto, G. P., Spivey, B. A., and A., P. D., "High-speed data acquisition in a diffraction tomography system employing large-scale toroidal arrays," *Int. J. Imag. Syst. Tech.* **8**, 137–147 (1997).

[12] Kornguth, P. J., Keefe, F. J., and Conaway, M. R., "Pain during mammography: characteristics and relationship to demographic and medical variables," *Pain* **66**(18), 187–194 (1996).

[13] Devaney, A. J., "A computer simulation study of diffraction tomography," *IEEE Trans. Bio. Eng.* **BME-30**(7), 377–386 (1983).

[14] Bamler, R. and Hartl, P., "Synthetic aperture radar interferometry," *Inverse Probl.* **14**, R1–54 (1998).

[15] Kak, A. C. and Slaney, M., [*Principles of computerized tomographic reconstruction*], IEEE Press, New York (1998).

[16] Born, M. and Wolf, E., [*Principles of Optics*], Cambridge University Press, Cambridge (1999).

[17] Wolf, E., "Three-dimensional structure determination of semi-transparent objects from holographic data," *Opt. Commun.* **1**, 153–156 (1969).

[18] Simonetti, F. and Huang, "From beamforming to diffraction tomography," *J. Appl. Phys.* **103**, 103110 (2008).

[19] Watson, G. N., [*The theory of Bessel Functions*], Cambridge, London, New York (1952).

[20] Anderson, V. C., "Sound scattering from a fluid sphere," *J. Acoust. Soc. Am.* **22**(4), 426–431 (1949).